Fabrication of sub-10 nm gap arrays over large areas for plasmonic sensors

T. Siegfried,[1,a)] Y. Ekinci,[1,2] H. H. Solak,[3] O. J. F. Martin,[4] and H. Sigg[1]
[1]*Laboratory for Micro- and Nanotechnology, Paul Scherrer Institut, 5232 Villigen-PSI, Switzerland*
[2]*Department of Materials, Laboratory of Metal Physics and Technology, ETH Zurich, 8093 Zurich, Switzerland*
[3]*Eulitha AG, 5232 Villigen PSI, Switzerland*
[4]*Nanophotonics and Metrology Laboratory, EPFL, 1015 Lausanne, Switzerland*

(Received 8 November 2011; accepted 3 December 2011; published online 27 December 2011)

We report a high-throughput method for the fabrication of metallic nanogap arrays with high-accuracy over large areas. This method, based on shadow evaporation and interference lithography, achieves sub-10 nm gap sizes with a high accuracy of ±1.5 nm. Controlled fabrication is demonstrated over mm^2 areas and for periods of 250 nm. Experiments complemented with numerical simulations indicate that the formation of nanogaps is a robust, self-limiting process that can be applied to wafer-scale substrates. Surface-enhanced Raman scattering (SERS) experiments illustrate the potential for plasmonic sensing with an exceptionally low standard-deviation of the SERS signal below 3% and average enhancement factors exceeding 1×10^6. © *2011 American Institute of Physics*. [doi:10.1063/1.3672045]

Surface plasmon-based sensing techniques have generated substantial interest especially since the demonstration of single molecule sensitivity in 1997.[1,2] This enhancement phenomenon relies on strongly confined electromagnetic fields generated by localized plasmons on metal nanostructures much smaller than the incident wavelength.[3,4] However, surface enhanced (SE) spectroscopic techniques are not yet routinely used at the industrial level. This is due to poor signal reproducibility, moderate average enhancement factors, and high costs.[5] To increase the signal enhancement, nanogap patterns are currently used: they produce extremely large electromagnetic fields for nano objects separated by a distance below 20 nm.[6] Local enhancement factors up to $\sim 10^9$ have been reported with a one-dimensional (1D) nanogap pattern,[7] enabling single molecule detection.[8] The fabrication of nanogap arrays has been demonstrated with a variety of techniques. Electron-beam lithography (EBL) is used for direct writing[9] or patterning of shadow masks for angular evaporation.[10,11] With EBL, the pattern can be designed and realized with an exceptional degree of freedom. Due to proximity effects of the electron beam and limitations set by the photoresist liftoff, the resulting metal nanogap dimensions are limited to above roughly 10 nm and a metal layer thickness of below 30 nm.[9,12] The serial writing process of EBL makes this technique unfavorable for the fabrication of large area and low-cost sensors. Other lithography-based techniques have been used, including molecular rulers[13,14] or atomic layer deposition (ALD),[7] as effective methods to tune the nanogap size even below 2 nm. This, however, involves complicated multistep fabrication processes and produces local defects, which are found to cause fluctuations of the surface-enhanced Raman scattering (SERS) enhancement across the sensing area[7] or between different substrates.

In this letter, we report the fabrication of homogeneous sub-10 nm gap arrays with high surface densities and over large areas. The fabrication scheme for our nanogap arrays consists of only two stages, lithography and metal layer deposition.

In the first step, extreme ultraviolet interference lithography (EUV-IL) is used to provide a 1D line array on the substrate, which is typically float glass or silicon. Details of the EUV lithography, available at the Swiss Light Source, can be found elsewhere.[15] This technique provides high resolution patterns over large areas and with high throughput. Briefly, a coherent beam with 13.5 nm wavelength is incident on a mask comprising two identical gratings. Beams diffracted by the gratings interfere to form high resolution patterns with dimensions below 10 nm half pitch.[16] In our experiments, line patterns with a period of 250 nm were exposed into a 80 nm thick hydrogen silsesquioxane (HSQ) photoresist layer. In a single exposure, a 1.7 × 0.6 mm^2 pattern was generated within a timeframe of 3 s–10 s, depending on the desired duty cycle. HSQ was then developed in a 25% tetra-methyl-ammonium-hydroxide (TMAH) solution for 60 s. After the exposure, HSQ is cross-linked to form a SiO_x network providing a chemically stable pattern that was used directly without further etching into the substrate.

In the second step, glancing angle deposition (GLAD) is used to thermally evaporate metal layers directly onto the photoresist pattern, as illustrated in Fig. 1. A similar process was

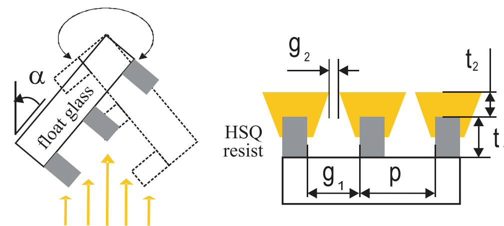

FIG. 1. (Color online) Scheme of the shadow evaporation process. The metal is evaporated iteratively from two sides of the surface.

[a)]Author to whom correspondence should be addressed. Electronic mail: thomas.siegfried@psi.ch.

 © 2011 American Institute of Physics

previously used to obtain metal nanowire arrays.[17,18] However, sub-10 nm gap arrays with excellent homogeneity over large surfaces have not yet been reported. Gold and chromium, both of 99.99% purity, were deposited at angles α between 30° and 70° from the surface normal and with an azimuthal orientation perpendicular to the length of the nanowires (Fig. 1). Repeated cycles of ~4 nm metal layer deposition (at a rate of 0.3 nm/s) followed by flipping the substrate to the opposite direction (Fig. 1) were carried out until the final thickness was reached. Important for our experiment is the observation that the linear slope of the gap edge changes for a separation distance smaller than roughly 30 nm. Beyond this distance, the gap closes only slowly when additional metal is deposited (see, for example, Fig. 2(b)).

Ballistic Monte Carlo simulations[19] were performed to analyze the geometry resulting from this GLAD process. Using a 2D home-made code, the trajectory and sticking of single metal particles with a 0.7 nm size were simulated. The particles were impinging on the surface from random positions under a specified angle. Similar to the experiment, the angle of the trajectory was flipped after a certain deposition time. Once a particle reached the uppermost surface, a diffusion length was introduced to model the further movement of the particle on the surface which controls the filling up of pores underneath.

In the first example, we have evaporated chromium. From the SEM images in Fig. 2(a), one can clearly see a columnar shaped layer growth that is known to result from angular evaporation and an exceptionally low diffusion length of the material.[20] Interestingly, no closure of the gap was observed, even for metal thicknesses exceeding 160 nm. Instead, self shadowing of the adjacent geometry seemed to prevent the gap from closing, making possible the realization of sub-10 nm gap sizes in a very reliable manner (see, for example, Fig. 2(b)). In the simulations, the diffusion length was set to 0, according to the small effective diffusion length of chromium. This assumption reproduced the experimentally observed geometry and the columnar growth very well, as illustrated by comparing Figs. 2(b) and 2(c).

Gold was used as another example, which was selected for subsequent SERS studies due to its tunable plasmon resonance in the visible range, chemical inertness, and biocompatibility.[21] As opposed to chromium, gold forms much larger grains during deposition (Figs. 3(a) and 3(b)) and does not form films with columnar texture thanks to a remarkably high diffusion length of the adatoms.[22] Again, we observed an initial almost linear closing of the gap that gradually slowed down once the gap was below 30 nm. In the ballistic simulation, an effective diffusion length of 2.1 nm was used, to account for the surface diffusion. The simulated cross section reproduced the experimental geometry very well, as illustrated in Fig. 3(b). Furthermore, the simulation model was used to predict the size of the nanogap arrays and its dependence on the evaporation angle, gold layer thickness, and HSQ line width. Experimental control of the final gap size was obtained by varying the initial HSQ gap size. For Au gap sizes down to roughly 10 nm, we could obtain extremely high uniformity of the patterned area with an accuracy of ±1.5 nm, as indicated in Fig. 3. This homogeneity was reduced for gap sizes below 10 nm, when crystallites from opposite sidewalls start randomly to coalesce.

Thanks to the shadowing effect, the formation of nanogaps was found to be self limited, enabling the control of the evaporation process accurately. In a typical evaporation process, up to 8 single substrate chips were coated simultaneously, covering a 4 in. substrate. With an appropriate low-cost lithography tool, e.g., displacement Talbot lithography[23] or laser interference lithography,[24] one could easily pattern and evaporate nanogap arrays over a full wafer, which was, however, not a part of this study.

The SERS enhancement provided by the fabricated nanogap arrays was evaluated using spectra recorded on a Horiba LabRam HR device (Fig. 4(a)). The excitation source was a 633 nm HeNe laser with 2 mW power collimated by a

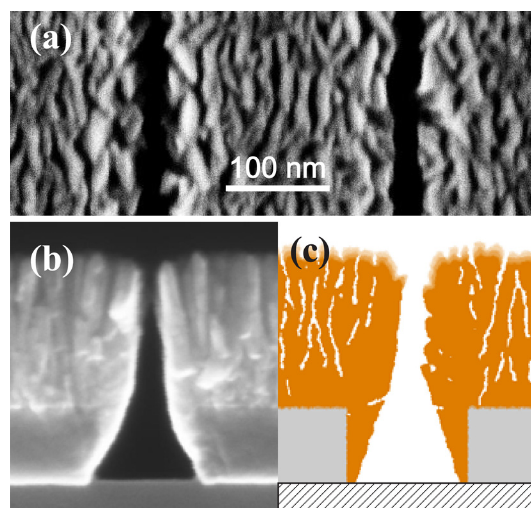

FIG. 2. (Color online) (a) Top view SEM and (b) cross sectional view of a cleaved chromium nanogap array compared with (c) ballistic simulation results. The 160 nm thick metal was evaporated at an angle of 55° from the surface normal. The resulting gap size is ~10 nm. The underlying pattern consists of the HSQ photoresist with a periodicity of 250 nm, a thickness of 80 nm, and a gap size of 110 nm. Silicon was used as a substrate.

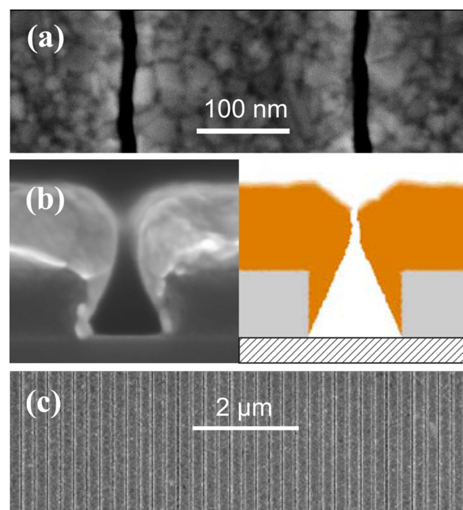

FIG. 3. (Color online) (a) and (c) Top view SEM and (b) cross sectional view of a cleaved gold nanogap array compared with ballistic simulation results. The 100 nm thick metal was evaporated at an angle of 60° from the surface normal. The resulting gap size is ~13 nm. The underlying pattern consists of the HSQ photoresist with a periodicity of 250 nm, a thickness of 80 nm, and a gap size of ~110 nm. Silicon was used as a substrate.

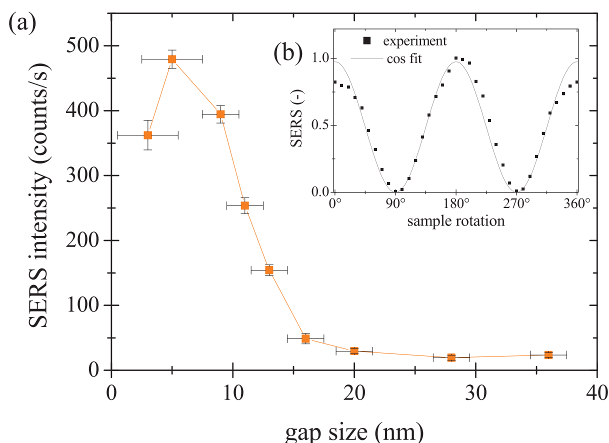

FIG. 4. (Color online) (a) SERS intensity for varying nanogap size. (b) SERS intensity as a function of the sample rotation for linearly polarized excitation. The sample consists of a nanogap array with a Au thickness of 100 nm. The excitation was at 633 nm and the SERS intensity corresponded to the 1008 cm^{-1} peak of a self assembled benzeneethanethiol monolayer. Error bars correspond to the standard deviation of 16 spatially separated SERS measurements and quantitative analysis of SEM images across the patterned area.

50X (NA of 0.5) objective. The SERS intensity was found to increase strongly for gap sizes below 20 nm, as expected. Within the $500 \times 400\,\mu m^2$ sensing area, the SERS signal was found to be highly reproducible with a standard deviation below 3%. For a 10 nm gap array, we have calculated an average enhancement factor of 1×10^6, with Raman spectra recorded from an undiluted analyte solution.

For gap sizes below ~10 nm, the SERS intensity leveled out and decreased for gap sizes below ~5 nm, as illustrated in Fig. 4(a). This discrepancy from the expected trend can be explained by increasing the events of coalescing gap sidewalls. This was not only found to reduce the overall SERS signal, but also to increase the areal standard deviation to roughly 6%.

The SERS intensity exhibited clear polarization dependence with maximal values for the electric field perpendicular to the nanogap expansion, as shown in the inset of Fig. 4(b). This large intensity ratio between s- and p-polarizations, indicates a well defined enhancement mechanism located within the nanogap and excludes the contributions from surface roughness.

In summary, we have fabricated sub-10 nm gap arrays with a simple, self-aligning, and easily scalable shadow evaporation technique. The formation of nanogaps was supported by simulations and could be realized with high homogeneity as observed both in SEM images and SERS measurements, with signal deviations below 3%. The potential use as a SERS sensor was demonstrated, with an average enhancement factor of 1×10^6 well reproducible over the entire patterned sensing area. Such patterns have great potential for numerous applications ranging from sensors to nanoliter vessels and nano-membranes.

The work was supported by the Swiss Federal Foundation. Part of this work was performed at the Swiss Light Source (SLS), PSI, Switzerland. We acknowledge the support of M. Vockenhuber for EUV lithography and P. Sahoo for preliminary experiments.

[1] K. Kneipp, Y. Wang, H. Kneipp, L. T. Perelman, I. Itzkan, R. R. Dasari, and M. S. Feld, Phys. Rev. Lett. **78**, 1667 (1997).
[2] S. Nie and S. R. Emory, Science **275**, 1102 (1997).
[3] S. J. Tan, M. J. Campolongo, D. Luo, and W. Cheng, Nat. Nanotechnol. **6**, 268 (2011).
[4] M. Rycenga, C. M. Cobley, J. Zeng, W. Li, C. H. Moran, Q. Zhang, D. Qin, and Y. Xia, Chem. Rev. **111**, 3669 (2011).
[5] M. J. Natan, Faraday Discuss. **132**, 321 (2006).
[6] J. Zuloaga, E. Prodan, and P. Nordlander, Nano Lett. **9**, 887 (2009).
[7] H. Im, K. C. Bantz, N. C. Lindquist, C. L. Haynes, and S.-H. Oh, Nano Lett. **10**, 2231 (2010).
[8] A. Otto, J. Raman Spectrosc. **37**, 937 (2006).
[9] H. Duan, H. Hu, K. Kumar, Z. Shen, and J. K. W. Yang, ACS Nano **5**, 7593 (2011).
[10] W. Zhu, M. G. Banaee, D. Wang, Y. Chu, and K. B. Crozier, Small **7**, 1761 (2010).
[11] R. Stosch, F. Yaghobian, T. Weimann, R. J. C. Brown, M. J. T. Milton, and B. Güttler, Nanotechnology **22**, 105303 (2011).
[12] H. Duan, V. R. Manfrinato, J. K. W. Yang, D. Winston, B. M. Cord, and K. K. Berggren, J. Vac. Sci. Technol. B **28**, C6H11 (2010).
[13] G. S. McCarty, Nano Lett. **4**, 1391 (2004).
[14] R. Negishi, T. Hasegawa, K. Terabe, M. Aono, T. Ebihara, H. Tanaka, and T. Ogawa, Appl. Phys. Lett. **88**, 223111 (2006).
[15] V. Auzelyte, C. Dais, P. Farquet, D. Grutzmacher, L. J. Heyderman, F. Luo, S. Olliges, C. Padeste, P. K. Sahoo, T. Thomson *et al.*, J. Micro/Nanolith. MEMS MOEMS **8**, 021204 (2009).
[16] B. Päivänranta, A. Langner, E. Kirk, C. David, and Y. Ekinci, Nanotechnology **22**, 375302 (2011).
[17] V. Auzelyte, H. H. Solak, Y. Ekinci, R. MacKenzie, J. Vörös, S. Olliges, and R. Spolenak, Microelectron. Eng. **85**, 1131 (2008).
[18] J. G. Bai, W. H. Yeo, and J. H. Chung, Lab Chip **9**, 449 (2009).
[19] S. Müller-Pfeiffer, H. van Kranenburg, and J. C. Lodder, Thin Solid Films **213**, 143 (1992).
[20] K. Naoto, E. Akinori, O. Kiyoshi, S. Ippei, S. Yuichi, and M. Shoji, J. Vac. Sci. Technol. A **19**, 153 (2001).
[21] M. Moskovits, J. Raman Spectrosc. **36**, 485 (2005).
[22] T. Ishida, Y. Nakajima, J. Endo, D. Collard, and H. Fujita, Nanotechnology **20**, 065705 (2009).
[23] H. H. Solak, C. Dais, and F. Clube, Opt. Express **19**, 10686 (2011).
[24] C. Lu and R. H. Lipson, Laser Photonics Rev. **4**, 568 (2009).